Advanced Industrial and Engineering Polymer Research 9 (2026) 100266

Contents lists available at ScienceDirect

Advanced Industrial and Engineering Polymer Research

journal homepage: http://www.keaipublishing.com/aiepr

Research paper

Valorization of end-of-life wind blades in alkyd anticorrosion coatings through an open-loop chemical recycling

Stefano Turri [a,*], Valeria De Fabritiis [a], Gianmarco Griffini [a], Tania Trombetta [b], Andrea Cristoforetti [c], Michele Fedel [c]

[a] Department of Chemistry, Materials and Chemical Engineering "Giulio Natta", Politecnico di Milano, Piazza Leonardo da Vinci 32, 20133, Milan, Italy
[b] N. Benasedo S.P.A, Via Asiago 332, 21042, Caronno Pertusella, Italy
[c] Department of Industrial Engineering, University of Trento, Via Sommarive 9, 38123, Trento, Italy

ARTICLE INFO

Article history:
Received 25 March 2026
Received in revised form
23 June 2026
Accepted 21 July 2026

Keywords:
Chemical recycling
Composite materials
Alkyd resin
Anticorrosion
Electrochemical impedance spectroscopy
Circular economy

ABSTRACT

This work proposes the development of modified alkyd coatings based on the open-loop chemical recycling of fiber-reinforced polymer (FRP) composites from end-of-life (EoL) wind turbine blades. Epoxy-based glass FRP composites are efficiently depolymerized by a catalyst-assisted mild solvolysis process using a biobased diol, achieving complete resin dissolution and recovery of clean fibers. The resulting organic recyclate, rich in hydroxyl-terminated epoxy-derived oligomers, is directly employed - without further purification or modification steps - as a reactive macromer for the synthesis of industrial alkyd resins. Modified alkyds containing up to 17 wt% recycled fraction are formulated into pigmented anticorrosive coatings and applied on steel substrates. Comprehensive characterization shows that recyclate contents up to 10 wt% do not adversely affect coating processability, curing, mechanical properties, outdoor durability, or corrosion protection, as confirmed by electrochemical impedance spectroscopy. These results demonstrate a viable and scalable route for the high-value reuse of chemically recycled FRP materials in protective coatings, enabling a synergistic circular economy link between the wind energy and coatings industries.

© 2026 Kingfa Scientific and Technological Co. Ltd. Publishing services by Elsevier B.V. on behalf of KeAi Communications Co. Ltd. This is an open access article under the CC BY-NC-ND license (http://creativecommons.org/licenses/by-nc-nd/4.0/).

1. Introduction

Fiber-reinforced polymer composites (briefly, FRPs) are structural materials increasingly used in many manufacturing sectors due to their outstanding modulus-to-weight ratio and intrinsic environmental durability. They mostly consist of glass or carbon fibers associated with thermoset resins, like unsaturated polyesters and epoxies [1–4]. In spite of their appealing performances, a correct recycling of FRPs components at their end-of-life (EoL) is very challenging due to their multi-material composition. For this reason, a large fraction of FRPs is still destined to be landfilled or incinerated [5–7], in a way not compliant with the principles of the circular economy [8]. Currently, mechanical shredding and thermochemical methods, such as pyrolysis, are among the most consolidated recycling technologies of FRPs [7,9], despite the fact that they typically yield low-value recycled materials. In recent years, the scientific literature has however witnessed a growing interest towards chemical recycling by solvolysis in mild conditions [10–14]. The key advantages of this recycling technology are an efficient liberation of fibers with very good retention of their physical properties, making them suitable for the preparation of second-generation composites, and the recovery of an organic recyclate, containing the depolymerized oligomers, easier to separate and collect. However, a profitable exploitation of this organic fraction is still an open issue, as its conversion into a new resin system for FRPs remanufacturing, according to a closed-loop scenario, may require several chemical steps [12,15], making the overall process not economically sound.

Here, we present instead a different approach, consisting of a direct reuse of the organic fraction recyclate as "macromer" for the synthesis and modification of coating resins. We focused onto chemical recycling of FRPs made of glass and epoxy resins cured with anhydride, for two reasons: i) they represent the main FRPs material used for wind turbine manufacturing (one of the major sources of EoL composite waste [6,16–18] in the next years and

* Corresponding author.
E-mail address: stefano.turri@polimi.it (S. Turri).
Peer review under the responsibility of editorial board of Advanced Industrial and Engineering Polymer Research

https://doi.org/10.1016/j.aiepr.2026.07.001
2542-5048/© 2026 Kingfa Scientific and Technological Co. Ltd. Publishing services by Elsevier B.V. on behalf of KeAi Communications Co. Ltd. This is an open access article under the CC BY-NC-ND license (http://creativecommons.org/licenses/by-nc-nd/4.0/).

decades); ii) they can be efficiently solvolyzed by glycolysis under mild conditions with homogenous catalysis [10]. Due to the particular nature of the organic fraction recyclate (*i.e.*, rich in –OH functions), the latter can be used as a reactive intermediate, without any further purification step, for the chemical modification of different polyester-type coatings, such as alkyd resins. Along these lines, different alkyd-based coatings are developed in this study, by incorporating varying fractions of organic recyclate, in order to evaluate their technological properties, and particularly their behavior in the corrosion protection of low carbon steel.

2. Experimental section

2.1. Materials

Bisphenol A diglycidyl ether (DGEBA) epoxy resin, hexahydro-4-methylphthalic anhydride (HHMPA) as curing agent, 2-methylimidazole (2-MI) as accelerator for the curing, and 1,5,7-triazabicyclo [4,4,0]dec-5-ene (TBD) as transesterification catalyst were all purchased from Merck. Tetrahydrofuran (THF) purity grade 99%, and 1,3-propanediol (1,3-PD) were also purchased from Merck and used as received. Biaxial (0°/90°) glass fibers (GFs, diameter 16 μm and density 2.60 g/cm^3) were purchased from Mates Italiana and used for the manufacturing of FRPs composite. Fragments of EoL wind turbine blades based on glass fibers (GFs) and epoxy resins were kindly supplied by Haiki Cobat (Italy). Steel panels were purchased from Q-lab and used as substrate for coating deposition and testing.

2.2. Composite preparation and chemical recycling by catalyzed solvolysis

DGEBA was mixed with HHMPA as curing agent in 1:1 stoichiometric ratio and 2-MI as catalyst (0.5 wt% with respect to total mass) at 100 °C in a beaker. The homogeneous mixture was then poured into silicon molds and cured in a ventilated oven at 150 °C for 2 h to obtain the cured thermoset (Tg = 130 °C, DSC curve reported in Fig. S2 in the Supporting Information). The gel content of the cured epoxy resin (measured in THF) was >98%. The corresponding glass fibers reinforced anhydride-cured epoxy composite (GFRP) was obtained through vacuum-bag impregnation. The final GFRP was characterized by around 50 wt% GFs content and displayed homogeneous fiber impregnation (TGA curve reported in Fig. S3 in the Supporting Information). A catalyst-assisted mild glycolysis process was performed to solvolyze the GFRP samples, using 1,3-PD as solvent and TBD (3 wt%, computed with respect to the total amount of solvent and sample) as transesterification catalyst [10]. A two neck-flask was filled with the solvent, the GFRP sample, and the catalyst. The composite-to-solvent ratio was set to 40:100 by weight. The reaction was kept under magnetic stirring and heated at 180 °C for 2 h, under a static nitrogen atmosphere. At the end of the process, the GFs were completely liberated and separated by filtration. The homogeneous organic phase, containing the depolymerized epoxy oligomers and the solvent (*viz.*,1,3-PD), was used as it is for the chemical modification of the alkyd resin. The solvolysis process was validated also on the neat crosslinked epoxy (*e.g.*, with no fibers), and on real EoL wind turbine blades fragments, always observing a complete dissolution of the cured resin.

2.3. Chemical modification of alkyds with the organic recyclate

The alkyd resin used in this study as a benchmark was a standard industrial product obtained by polycondensation of fatty acids, phthalic anhydride, and a mixture of different bi- and tetrafunctional polyols, and it is used as anticorrosion paint. It will be indicated in the following as Alk-st resin. Typically, all the syntheses of the alkyd resins were carried out with a four-neck glass reactor provided with a stirrer, a thermometer, a cooler connected to a water collecting vessel, and an inert gas inlet. The reaction involved a two-stage polyesterification process, with progressive removal of water (by-product) through azeotropic distillation of xylene. The modifications on the benchmark Alk-st resin were obtained by the same process, keeping fixed the content of fatty acids and phthalic acid content, and adding different amounts (from 5 wt% to 17 wt%) of organic recyclate (composed by residual 1,3-PD and oligomeric structures) recovered from the solvolysis process to partially replace the polyol mixture, obtaining a series of modified alkyds indicated as Alk-x (where x represents the weight fraction of organic recyclate incorporated in the final resin system). In particular, the maximum recyclate content was limited to 17 wt%, which represents the higher incorporation level that could be employed in the alkyd resin formulation to avoid gelification phenomena during the polycondensation process. The comparative features of the standard alkyd system and of their modified versions are summarized in Table 1.

2.4. Alkyd coating formulation and curing

The different alkyd resins were formulated by high-speed mixing with TiO_2 (Deltio TX 81, from Hunstman, 40 wt% on solid resin) and using two different curing agents in an 8:2 (resin:curing agent) ratio, namely Cymel 325 (a melamine-based crosslinker, from Allnex) and Desmodur BL3125 (a blocked aliphatic polyisocyanate, from Covestro). The corresponding pigmented coatings were diluted to 50% solid, spray-applied on well cleaned cold rolled low carbon steel smooth panels (Italgard), and oven-cured at 150 °C for 30 min.

2.5. Characterization techniques

Fourier-transform infrared (FTIR) spectroscopy was performed using a Nicolet iS50 FTIR spectrometer equipped with a Specac Golden Gate ATR accessory. The FTIR spectra were collected in the range of 4000–600 cm^{-1} at a resolution of 4 cm^{-1} and 64 accumulated scans per sample. Gel permeation chromatography (GPC) analyses were performed using a Waters 486 Tunable Absorbance Detector, a Waters 515 HPLC pump (THF as mobile phase; flow rate 1 mL min^{-1}; T = 35 °C), and four columns (models HR 5, HR 4, HR 3, and HR 2), with polystyrene fractions as standards for calibration. ^{1}H nuclear magnetic resonance (NMR) spectrum was recorded on a Bruker Avance II 500 MHz in $CDCl_3$ solution. The acid number (mgKOH/g) was measured by chemical titration according to ASTM D1639. Viscosity measurements on the different resins were carried out with a Brookfield DV2T rotational viscometer at 25 °C. Differential scanning calorimetry (DSC) analyses were carried out with a Mettler-Toledo DSC/823e under nitrogen atmosphere to determine the glass transition temperature (Tg) of the resin systems. Thermogravimetric analyses (TGA) were performed with a TGA 550 apparatus (TA Instruments) to assess the cleanliness of the recycled fibers after the solvolysis process and to analyze the fiber content in the GFRPs. The sample under test was heated in a nitrogen atmosphere from 25 °C to 600 °C at a heating rate of 10 °C min^{-1}, to evaluate the weight loss in inert, oxygen-free, heating conditions. Scanning electron microscopy (SEM) imaging was employed to check the cleanliness of recycled fibers, using an EVO 50 series instrument (Carl Zeiss AG) operated under high vacuum using an electron high tension (EHT) of 20 kV and a probe current of 100 pA at 100x and 5000x magnification.

Table 1
Characteristics of standard alkyd (Alk-st) and modifications thereof (line 1 and 2) and corresponding application performances (line 3 and 4).

Resin characteristics	Alk-st	Alk-5%	Alk-10%	Alk-17%
Acid number	6–12 mgKOH/g	12 mgKOH/g	20 mgKOH/g	10.8 mgKOH/g
Dry content	70%	70.8%	60.2%	70.1%
Viscosity (25 °C)	3350 mPa s	2300 mPa s	2950 mPa s	3450 mPa s
Tg	3 °C	−5 °C	−6 °C	−18 °C

Solvent type: xylene for Alk-st and ethyl lactate for Alk-5%, Alk-10% and Alk-17%.
Aspect: clear.

2.6. Technological characterization of the coatings

MEK test was conducted to assess the chemical resistance of the alkyd coatings after curing according to ASTM D4752–20 [19]. Pull-off measurements were carried out to assess coating adhesion according to ASTM D4541, using a ARW-T05 equipment [20]. More specifically, a 20 mm diameter aluminum dolly was glued to the coating with a two-component epoxy adhesive (Scotch-Weld DP760, 3 M) and used to evaluate the adhesive strength (in MPa) of the coating on the steel substrate. Three replicates have been performed for each sample. The Wolff-Wilborn pencil-hardness test was performed according to ASTM D3363 [21]. The hardest pencil not scratching the coating surface was used as the coating hardness value. Contact angle measurements were used to assess the coating wettability using an Optical Contact Angle (OCA) 15plus set-up by Dataphysics. The test was run using a 500 μL Hamilton syringe filled with water. Profile extraction to determine the water contact angle (θ) was performed through Laplace-Young fitting. For each coating, 30 measurements have been performed. Gloss measurements at 60° were determined using a Spectro-guide type sphere glossmeter (BYK). For all the measurements, a minimum of five representative locations were selected on the coating surface, and the mean gloss value was reported. Color index measurements were performed using a 3nh model YS3010 spectrophotometer with a standard illuminant at an observation angle of 10° in terms of RGB coordinates. A minimum of five representative locations on the coating surface were selected for the recording, and the mean RGB values were reported.

2.7. Weathering tests

The coated panels were exposed to 2000 h of accelerated weathering in a QLAB accelerated weathering chamber model QUV/SE, using the following cycle: 4 h, 50 °C dark and 8 h, 60 °C with irradiation of 0.77 W/m^2.

2.8. Electrochemical impedance spectroscopy (EIS)

The dry film thickness of the cured coatings was controlled using a Elcometer magnetic thickness gauge on spare replicate panels prepared in the same batch, performing at least 10 measurements per formulation. The average thickness across all formulations was consistently maintained in the range of 27–34 μm, with no statistically significant deviations among the different recycled content additions (*e.g.*, Alk-st: 31.5 ± 2.0 μm; Alk-17%: 28.1 ± 2.5 μm). The coated samples were monitored by EIS under immersion in a 3.5 wt% NaCl solution. For each type of coating, including the reference, three different panels were selected, on which electrochemical cells filled with the electrolyte were fixed. The impedance measurements were performed over an exposed area of approximately 15 cm^2, with an AC perturbation amplitude of 15 mV. Measurements were recorded once per hour during the first 24 h of immersion, and additional evaluation was carried out up to 1000 h to assess the long-term behavior. The EIS spectra at 1 h, 2 h, 24 h, and 1000 h were also compared through equivalent circuit analysis for all replicas. All spectra acquired during the first 24 h exhibited a response characterized by a single time constant, for which the R (QR) model was selected. A constant phase element (CPE, Q) was introduced to account for deviations from ideal capacitive behavior, as evidenced by the depressed semi-circles in the Nyquist plots. The fitting parameters included the coating resistance (R), the CPE parameter (Q), and the exponent α associated with the CPE. The average values over the three replicas were plotted. Some spectra collected at 1000 h of immersion displayed a two-time constant behavior modeled in this case with an R (Q (R (QR))) circuit. In this situation, the fitting parameters attributed to the coating contribution were plotted as the evolution of the ones at shorter periods of immersion.

3. Results and discussion

The chemical recycling by solvolysis of epoxy-anhydride cured resins and their composites was recently described for the case of carbon FRPs (characterization and details of the resin are reported in Section S1 in the Supporting Information) [10,22]. Here, the process was also validated on GFRPs, using a biobased diol (namely, 1,3-PD) as solvent carrier. The solvolysis process was found to be very efficient in dissolving in mild conditions the epoxy network through a transesterification mechanism, releasing some OH-terminated species as shown in Fig. 1. Specifically, based on the reported literature [22], a possible catalytic mechanism for the epoxy depolymerization in –OH bearing solvent and TBD is proposed. First, TBD reacts with the ester linkages of the polymeric network *via* nucleophilic attack of both disubstituted nitrogen atoms at the carbonyl groups, obtaining a betaine-like intermediate. Hence, proton transfer on the protonated nitrogen leads to the formation of a TBD amide intermediate and the liberation of OH-containing species. In the presence of the solvent (*i.e.*, 1,3-PD), a new ester can be rapidly formed, allowing regeneration of TBD and completing a catalytic transesterification cycle. The diffusion of the TBD–glycol system into the epoxy network enables continuous catalytic cleavage of ester linkages throughout the material, resulting in efficient depolymerization of the epoxy resin.

After solvolysis, GFs were released free of resin residues, becoming potentially reusable for the remanufacturing of second-generation GFRP components (characterization data of the recycled GFs are reported separately in Fig. S4 in the Supporting Information).

On the other hand, the recovered organic fraction recyclate was a homogeneous and stable liquid phase, containing the depolymerized oligomers (see Fig. 1), the diol used as solvent carrier (*i.e.*, 1,3-PD), and the catalyst. The FTIR spectrum and typical GPC curve of the organic fraction recyclate are shown in Fig. 2a and b.

The FTIR spectrum reported in Fig. 2a shows a high intensity signal around 3300 cm^{-1}, attributable to the –OH stretching of the residual solvent (*e.g.*, 1,3-PD) and of the oligomeric products

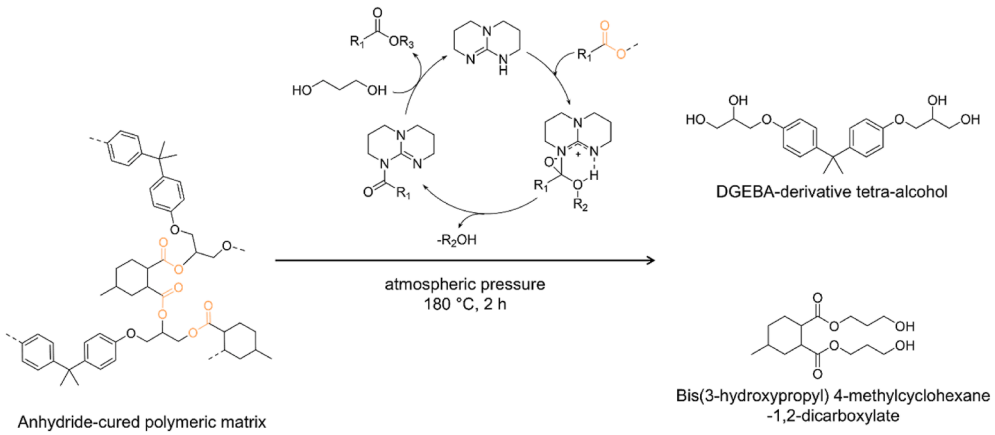


Fig. 1. The mechanism of dissolution of epoxy-anhydride networks through catalyst-assisted solvolysis, and the main oligomers formed [10,22].

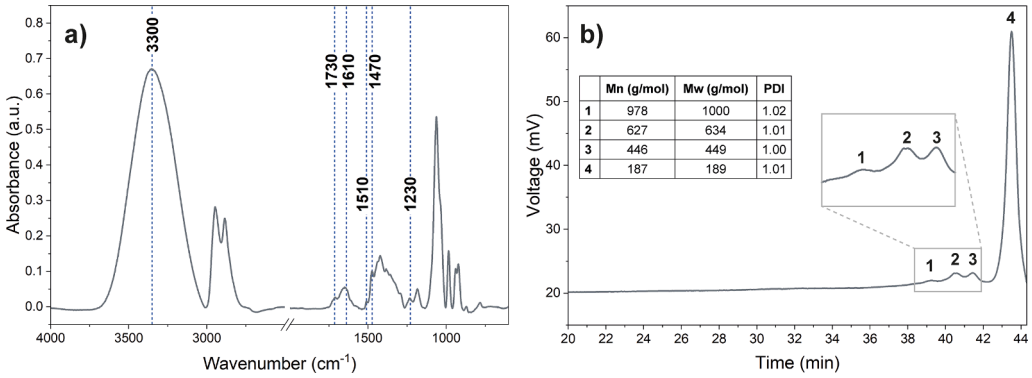


Fig. 2. a) FTIR spectrum and b) GPC curve of the organic fraction recyclate.

(reported in Fig. 1). Characteristic peaks are detected at around 1730 cm^{-1} and 1230 cm^{-1}, assigned to ester C=O and C–O stretching, respectively. Finally, the aromatic C=C stretching vibrations are represented to the peaks at 1610 cm^{-1}, 1510 cm^{-1} and 1470 cm^{-1}, confirming the presence of the DGEBA-derived oligomeric structure. In addition, the GPC analysis (Fig. 2b) allowed an estimation of the molecular weight and molecular weight distribution of the organic recyclate. Among them, the peak found at 43.5 min (label 4 in Fig. 2b), appearing at the longest retention time, can be associated with chemical structures related to the residual solvent (*i.e.*, 1,3-PD, 76 g/mol). For confirmation, the GPC analysis of the neat solvent is reported in Fig. S5 in the Supporting Information. Hence, the lower intensity peaks observed at 40.0 min and 40.6 min (labels 1, 2 in Fig. 2b, respectively) may be related to the DGEBA-derived oligomeric structures, while the peak observed at 41.4 min could be associated with the hexahydrophtalic-based ones, obtained from the depolymerization reaction (see Fig. 1).

Different amounts of organic recyclate were used in the polycondensation reactions to obtain the modified alkyd resins. Remarkably, no particular issues like acceleration/retardation effects on kinetics or gel formation were observed during the polymerization process, indicating the straightforward usability of the recovered fraction as effective reactive component for these polymeric systems (GPC analyses of the coating formulations are shown in Fig. 3). All the synthesized alkyd resins were pigmented with TiO_2, formulated with polyisocyanates or melamines as hardeners, spray-applied onto steel panels, and oven cured as reported in the experimental part.

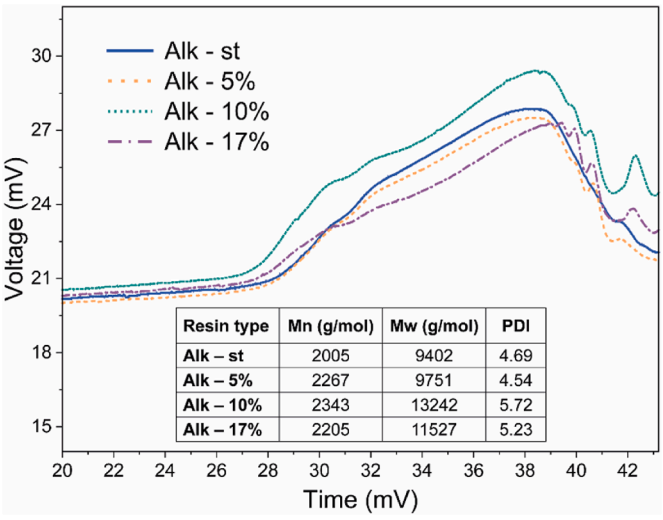


Fig. 3. GPC analyses of the standard and modified alkyd resins. Two replicates have been performed for each formulation. The table reports the average values of Mn, Mw and PDI of the main elution peak identified for all the formulations.

The comparison among the characteristics of the standard alkyd resin (Alk-st) and the corresponding modifications through the incorporation of the organic recyclate is shown in Table 1.

All the alkyd resins showed similar characteristics, with the partial exception of the sample Alk-10%, which is characterized by

a higher acid number than the other resins (20 mgKOH/g). Specifically, this value was intentionally accepted as the synthesis endpoint to limit further polyesterification and the associated viscosity increase, maintaining suitable resin processability. While the standard product was diluted with xylene, the modified resins (containing a higher fraction of biobased and recycled macromers) were diluted with a green solvent like ethyl lactate. The two solvents can be used in a quite interchangeable way. The results of the technological characterization of the corresponding cured coatings are reported in Table 2. Moreover, the resin Tg seems to decrease with increasing the recyclate content.

The alkyd coatings cured with polyisocyanates were found to exhibit slightly higher surface hydrophobicity and better adhesion onto steel, in comparison to the products formulated with melamines. The incorporation of different amounts of organic fraction recyclate appeared to have a little effect on the coating behavior, with a minor decrease of in the surface hardness, which was however found to be in line with the industrial benchmark. Additionally, the outdoor durability (expressed as retention of gloss after UV exposure to the weathering cycle) was not affected by the alkyd modification, and it was for all formulations comparable or superior to what was observed on the benchmark formulation.

A deeper investigation into the protective properties of the coatings was undertaken through electrochemical impedance spectroscopy (EIS) measurements. A representative example of spectra evolution in time is reported for each coating (Figs. 4 and 5). The Nyquist plots show a progressive and generalized decline in the barrier protection properties of the polyisocyanate-based alkyd coatings as the immersion time in the electrolyte increases. During the initial 24 h of exposure, all formulations exhibit high-impedance capacitive loops on the order of ~10^9–10^{10} Ω cm^2 for the 0.01 Hz impedance modulus, which indicates significant resistance to ionic transport through the coatings. A comparative observation of the four conditions reveals that the reference coating Alk-st (Fig. 4a) maintains the highest overall impedance in the very first hours of immersion, while the modification with recycled organic fractions leads to a limited but detectable reduction in the capacitive arc diameters, suggesting a slight increase in coating permeability. The performance after 1000 h of continuous immersion in the electrolyte are however very similar, regardless of the addition of recycled fraction.

The Nyquist plots provided in Fig. 5 illustrate the EIS monitoring of melamine-based alkyd coatings over a 1000 h immersion period in the electrolyte. This second set of results demonstrates more significant differences in barrier properties stability compared to the polyisocyanate-based systems, particularly regarding how the recycled organic fraction influences the barrier properties of the coatings for prolonged immersion time. During the entire duration of the exposure to the electrolyte, the reference coating Alk-st exhibits the most pronounced capacitive semi-circles with impedance modulus values at 0.01 Hz exceeding 10^{10} Ω cm^2. During the initial 24 h of immersion, the 5 wt% and 10 wt% recycled fraction (Fig. 5b,c) samples show a slightly lower impedance modulus values at 0.01 Hz compared to the reference. In particular, the 5 wt% recycled fraction sample shows an almost stable capacitive semi-circle during the entire immersion in the electrolyte. On the other hand, the addition of 17 wt% recycled fraction seems to be detrimental for the protection properties of the coatings, as demonstrated by the significantly less pronounced capacitive semi-circle shown in Fig. 5d.

The evolution of the electrochemical parameters extracted from the EIS fitting (Figs. 6 and 7) provides clear insights into the influence of the recycled organic fraction addition on the barrier properties of the different alkyd coatings. It is important to note that the points plotted in the EIS evolution graphs represent the average values derived from three independent macroscopic replicates. The standard deviation across these replicates, which captures the true sample-to-sample physical variability, was generally very low for the parameters representing bulk properties (within ±0.54% for α and ±15–30% for Q). Conversely, the variance for the pore resistance R was much broader (typically ±20–50%, increasing up to >100% at 1000 h for specific samples). This large relative deviation for R is physically justified and expected: while α and Q describe averaged volumetric behaviors, R is extremely sensitive to localized sub-microscopic defects. The formation of a single electrolyte permeation pathway in one replicate can drop its resistance by several orders of magnitude compared to the others. Because the physical degradation of R spans a logarithmic scale, its standard deviation among physical replicates appears mathematically large, reflecting a log-normal distribution of localized defects rather than poor measurement reproducibility. For all coatings, the constant phase element (CPE) exhibited α values close to 0.95 for all samples and immersion times, indicating a nearly ideal capacitive behavior and good dielectric homogeneity of the films [23]. This suggests that the incorporation of the recycled fraction does not significantly alter the capacitive nature of the coatings within the investigated concentration range. The analysis of the pore resistance (R), however, highlights some differences among the samples. In the polyisocyanate-based systems, the resistance remained comparable to that of the reference up to a 10 wt% addition of recycled material, maintaining high values around 10^{10} Ω cm^2. A further increase to 17 wt% resulted in a marked decrease of approximately one order of magnitude regardless of the immersion time, and this reduction was already evident at the early stages of exposure (Fig. 6). This behavior suggests that excessive incorporation of recycled material may alter the polymer network density or increase the free volume, thereby compromising the optimal sub-microscopic compactness and facilitating electrolyte permeation pathways, even in the

Table 2
Technological characterization of the white pigmented alkyd coatings. MEK test >100 d.r. for all the coating formulations.

Resin type	Hardener	Pencil hardness	Pull-off adhesion (MPa)	OCA (°)	Color (RGB)	Gloss (60°)	Gloss retention after 2000h[a] (%)
Alk-st	Desmodur	HB	2.03 ± 0.12	80 ± 6	R: 235; G: 237; B: 233	90	83
Alk-st	Cymel	B	1.55 ± 0.19	80 ± 5	R: 235; G: 237; B: 231	84	93
Alk-5%	Desmodur	HB	2.27 ± 0.30	82 ± 4	R: 233; G: 236; B: 233	88	93
Alk-5%	Cymel	2 B	1.24 ± 0.17	87 ± 1	R: 235; G: 236; B: 230	81	100
Alk-10%	Desmodur	B	2.88 ± 0.21	95 ± 2	R: 235; G: 236; B: 228	86	83
Alk-10%	Cymel	2 B	1.78 ± 0.06	88 ± 2	R: 236; G: 238; B: 234	85	85
Alk-17%	Desmodur	3 B	2.14 ± 0.10	92 ± 4	R: 232; G: 233; B: 225	86	84
Alk-17%	Cymel	5 B	1.08 ± 0.08	86 ± 1	R: 237; G: 233; B: 222	80	90

[a] Weathering test as described in the Experimental section.

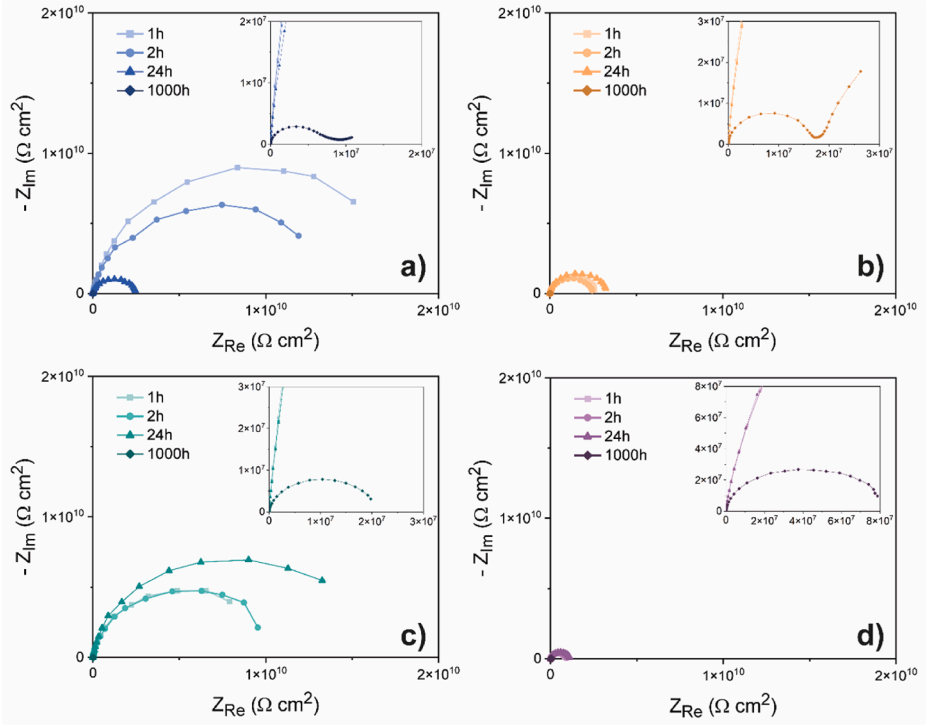


Fig. 4. EIS monitoring of polyisocyanate-based alkyd coatings on steel during immersion in 3.5 wt% NaCl solution for up to 1000 h: a) reference (Alk-st); b) 5 wt%; c) 10 wt% and d) 17 wt% of organic fraction recycled.

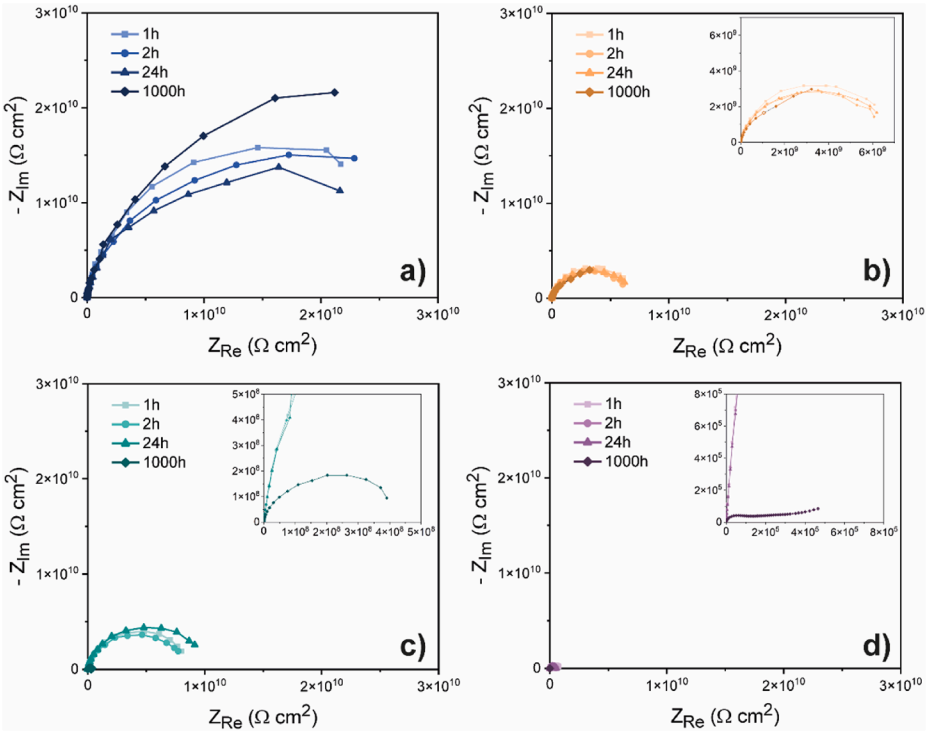


Fig. 5. EIS monitoring of melamine-based alkyd coatings on steel during immersion in 3.5 wt% NaCl solution for up to 1000 h: a) reference (Alk-st); b) 5 wt%; c) 10 wt% and d) 17 wt% of organic fraction recycled.

absence of macroscopic phase separation. It is worth noting that the raw EIS parameters were normalized by the exposed cell area (15 cm^2) but not by the film thickness. Since the pore resistance scales linearly with thickness, the minor micrometric variations among the sprayed samples are entirely negligible compared to the massive drop in R (one to two orders of magnitude) observed for the 17 wt% formulations. This confirms that the impedance degradation is fundamentally driven by the altered polymeric

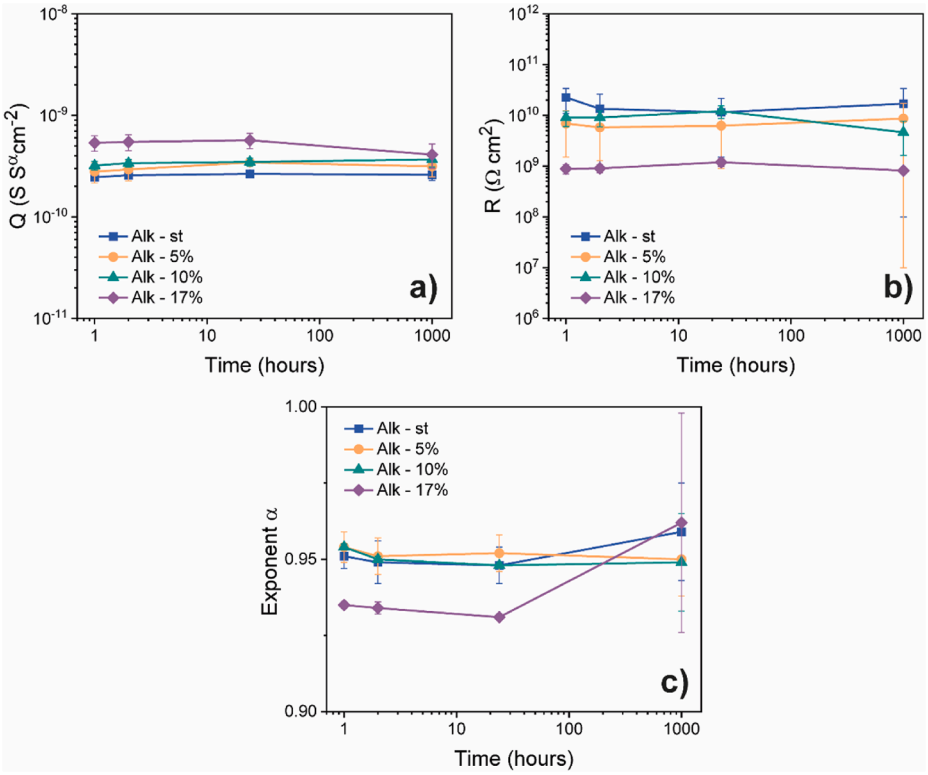


Fig. 6. Evolution of the electrochemical fitting parameters obtained from the equivalent circuits for polyisocyanate-based coatings during 1000 h of immersion: (a) constant phase element parameter (Q), (b) coating pore resistance (R), and (c) constant phase element (CPE) exponent (α). The error bars represent the standard deviation of the measurements.

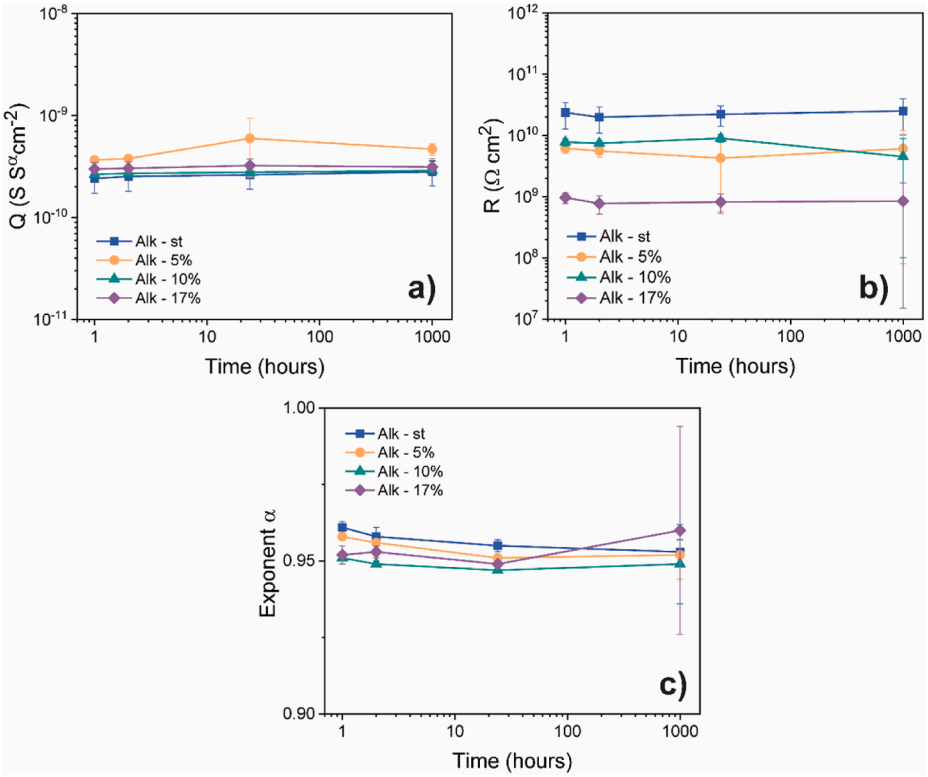


Fig. 7. Evolution of the electrochemical fitting parameters obtained from the equivalent circuits for melamine-based coatings during 1000 h of immersion: (a) constant phase element parameter (Q), (b) coating pore resistance (R), and (c) constant phase element (CPE) exponent (α). The error bars represent the standard deviation of the measurements.

network rather than geometric discrepancies. A different trend was observed for the melamine-based coatings (Fig. 7). In this case, the reference sample exhibited higher resistance values compared to the polyisocyanate system, confirming its inherently superior barrier performance. Nevertheless, even the addition of 5 wt% recycled material led to a reduction in R below the 10^{10} Ω cm^2 threshold, and the resistance remained at similar levels upon increasing the recycled fraction to 10 wt%. A further drop was observed at 17 wt% recyclate incorporation, where R fell below 10^9 Ω cm^2. As for the polyiscocyanate systems, these differences were already evident during the initial hours of immersion and remained stable up to 1000 h, suggesting that the recycled content primarily affects the initial coating structure rather than its long-term evolution. Nevertheless, despite the observed gap compared to the reference, the recorded pore resistance values remain satisfactory and are characteristic of a functional protective coating, in agreement with literature benchmarks for similar systems [24–26]. This performance is particularly significant given the relatively low film thickness of the single coating layer (approximately 30 μm), a condition that typically facilitates electrolyte diffusion in the presence of chlorides, thus confirming the effective barrier properties provided by these coatings [27,28]. Regarding the CPE parameter Q, no clear trend with the recycled content was observed. The values ranged between 10^{-9} and 10^{-10} S $S^{\alpha}\cdot cm^{-2}$, remaining comparable for all samples. Unlike the pore resistance, the Q parameter did not exhibit a significant evolutionary trend over time, remaining roughly constant within 10^{-9} and 10^{-10} S $s^{\alpha}\cdot cm^{-2}$. For this reason, Q could not be directly correlated to a progressive water uptake behavior, which typically evolves with immersion time. The rapid stabilization of Q suggests an immediate water saturation of the polymeric free volume. Furthermore, following the guidelines of Orazem and Tribollet [29], an effective capacitance was not extracted from Q. Such conversion requires assuming specific 2D or 3D time-constant distributions (*e.g.*, through Brug or Hsu-Mansfeld relationships), which would introduce arbitrary assumptions for these complex recycled polymer networks. Thus, interpreting the direct evolution of Q provides a more reliable phenomenological description of the coating's dielectric stability. After approximately 1000 h of immersion, a convergence of Q values was detected for all coatings. This behavior could be attributed to water saturation within the film and a subsequent stabilization of its dielectric response [30,31]. Alternatively, it may result from internal defect redistribution or partial polymer chain rearrangement during prolonged exposure, leading to a more homogeneous electrochemical response across the systems [32].

Overall, the results indicate that the incorporation of recycled material can be tolerated up to a certain threshold without compromising the coating barrier properties. However, excessive additions may lead to an early reduction in coating resistance, likely associated with sub-microscopic variations in the network cross-linking density that lead to the formation of preferential electrolyte diffusion pathways, while the overall dielectric homogeneity (α~0.95) and macroscopic appearance remain preserved.

4. Conclusive remarks

It has been estimated that EoL onshore wind turbine blades in the EU will reach more than 50,000 t/y in the coming years, with a cumulative total of 350,000–400,000 t by 2030 [33]. At present, decommissioned wind turbine blades are mainly diverted to cement kilns for energy recovery [34], a practice that is not fully compliant with circular economy principles.

Within this context, this work suggests an innovative pathway toward a synergistic circular economy of the wind energy sector with the metal coating industry, as an alternative scenario for the EoL treatment of wind turbine blades. Considering a solvolysis process performed as described in this study, and assuming a GF content of approximately 60 wt% in current-generation wind blades, it can be estimated that the chemical recycling of wind turbine blades could generate an annual flow of about $(50{,}000 \times 0.4) = 20{,}000$ t/y of depolymerized resin, corresponding to a total organic recyclate stream of approximately 145,000 t/y. While the recovered fibers can be reused as secondary raw materials for the manufacturing of second-generation composite products, this work demonstrates that the organic fraction can be directly exploited – without additional complex and costly separation or refining steps – as a reactive macromer for the modification of alkyd resins. Importantly, the experimental findings reveal that incorporation of recycled material during the resin synthesis is viable up to a threshold of approximately 10 wt%, without compromising the barrier properties and the other performances of the coating. Beyond that limit, an apparent reduction in coating resistance occurs. This premature failure is likely driven by microstructural changes or by the formation of preferential electrolyte diffusion pathways during long-term immersion.

Table 3
Global and EU market of the paint and coating sector.

Market segment (2024)	Region	Estimated volume	Estimated alkyd share
Total paint & coatings	Global	~58.2 Mt	~30% (total resins)
Industrial metal coatings	Global	~16.3 Mt	20%
Total paint & coatings	Europe (EU+)	~7 Mt	18%
Industrial metal coatings	Europe (EU+)	~1.9 Mt	15%
Alkyd resins (industrial focus)	Global	~2.4 Mt	–

Overall, the proposed technology enables an efficient reuse of all recycled fractions derived from FRPs, within a zero-waste framework. The potential economic impact of this scenario can be assessed by considering some key figures from the global and European paints and coatings markets [35–38], with particular emphasis on alkyd-based systems, as shown in Table 3.

The European metal coating sector accounts for approximately 1.9 Mt/y, of which about 15% (~285,000 t/y) consists of alkyd resins. This value is of the same order of magnitude as the potential organic recyclate stream generated from EoL wind turbine blade solvolysis (~145,000 t/y), thereby highlighting a strong potential synergy between the two industrial sectors, at least at EU level.

Further research is required to optimize both the chemical recycling process, particularly with respect to the selection of the most suitable solvent carriers, and the chemical modification strategies for different resin classes, with the aim of simultaneously enhancing coating performance and increasing the level of recyclate incorporation. Nevertheless, this proof-of-concept study demonstrates an effective way to turn an economic and societal challenge (EoL management of FRPs) into an industrial opportunity (more sustainable polymer coatings), promoting symbiotic cooperation between different market sectors through the guiding principles of the circular economy.

CRediT authorship contribution statement

Stefano Turri: Supervision, Formal analysis, Conceptualization. **Valeria De Fabritiis:** Data curation. **Gianmarco Griffini:**

Investigation, Funding acquisition. **Tania Trombetta:** Validation. **Andrea Cristoforetti:** Investigation. **Michele Fedel:** Supervision, Formal analysis.

Data availability

Data will be made available on request.

Conflict of competing interest

The authors declare the following personal relationship which may be considered as potential competing interests: Tania Trombetta is currently employed by N. Benasedo S.P.A, Via Asiago 332, 21042, Caronno Pertusella, Italy.

Acknowledgments

This research project has received funding from the European Union's Horizon Europe Research and Innovation Programme (grant agreement no. 101,058,756 – project: RECREATE), and from Lombardy Region (project EcoCirc, Accordo di collaborazione per la realizzazione di un'innovativa infrastruttura pilota regionale di supporto alla transizione verso l'economia circolare).

Appendix A. Supplementary data

Supplementary data to this article can be found online at https://doi.org/10.1016/j.aiepr.2026.07.001.

References

[1] M. Rani, P. Choudhary, V. Krishnan, S. Zafar, A review on recycling and reuse methods for carbon fiber/glass fiber composites waste from wind turbine blades, Compos. B Eng. 215 (2021) 108768.
[2] B. De, M. Bera, D. Bhattacharjee, B.C. Ray, S. Mukherjee, A comprehensive review on fiber-reinforced polymer composites: raw materials to applications, recycling, and waste management, Prog. Mater. Sci. 146 (2024) 101326.
[3] S. Karuppannan Gopalraj, T. Kärki, A review on the recycling of waste carbon fibre/glass fibre-reinforced composites: fibre recovery, properties and life-cycle analysis, SN Appl. Sci. 2 (2020).
[4] A.E. Krauklis, C.W. Karl, A.I. Gagani, J.K. Jørgensen, Composite material recycling technology—state-of-the-art and sustainable development for the 2020s, J. Compos. Sci. 5 (2021).
[5] C. Branfoot, H. Folkvord, M. Keith, G.A. Leeke, Recovery of chemical recyclates from fibre-reinforced composites: a review of progress, Polym. Degrad. Stabil. 215 (2023).
[6] J. Zhang, V.S. Chevali, H. Wang, C.-H. Wang, Current status of carbon fibre and carbon fibre composites recycling, Compos. B Eng. 193 (2020) 108053.
[7] D. Borjan, Ž. Knez, M. Knez, Recycling of carbon fiber-reinforced composites— difficulties and future perspectives, Materials 14 (2021).
[8] K. Winans, A. Kendall, H. Deng, The history and current applications of the circular economy concept, Renew. Sustain. Energy Rev. 68 (2017) 825–833.
[9] E. Morici, N.T. Dintcheva, Recycling of thermoset materials and thermoset-based composites: challenge and opportunity, Polymers 14 (2022).
[10] E. Manarin, O. Boumezgane, A. Giannino, V. De Fabritiis, G. Griffini, S. Turri, Towards a zero-waste chemcycling of thermoset polymer composites: catalyst assisted mild solvolysis for clean carbon fiber liberation and circular coating development, Sustain. Mater. Technol. 41 (2024).
[11] V. De Fabritiis, L. Matta, G. Griffini, S. Turri, Optimization of a chemical recycling process for epoxy-amine thermosets and their carbon fiber reinforced composites using a design of experiments approach, Clean. Eng. Technol. 26 (2025) 100988.
[12] C. Hao, B. Zhao, L. Shao, Y. Cao, M. Fei, W. Liu, T. Liu, Y.C. Chang, K.L. Simmons, J. Zhang, Mild chemical recycling of carbon fiber-reinforced epoxy composites in aqueous buffers and development of hydrothermally recyclable vitrimer composites from recyclates, Resour. Conserv. Recycl. 207 (2024).
[13] Y. Liu, Z. Yu, B. Wang, P. Li, J. Zhu, S. Ma, Closed-loop chemical recycling of thermosetting polymers and their applications: a review, Green Chem. 24 (2022) 5691–5708.
[14] Y. Wang, X. Cui, H. Ge, Y. Yang, Y. Wang, C. Zhang, J. Li, T. Deng, Z. Qin, X. Hou, Chemical recycling of carbon fiber reinforced epoxy resin composites via selective cleavage of the carbon-nitrogen bond, ACS Sustain. Chem. Eng. 3 (2015) 3332–3337.
[15] S.K. Kristensen, A. Ahrens, B.S. Donslund, T. Skrydstrup, Perspective on the development of monomer recovery technologies from plastics designed to last, ACS org, Inorg. Au 4 (2024) 373–386.
[16] M.J. Keith, B. Al-Duri, T.O. McDonald, G.A. Leeke, Solvent-based recycling as a waste management strategy for fibre-reinforced polymers: current state of the art, Polymers 17 (2025) 843.
[17] A. Fresneda Cruz, C. Chaine, M.B. Figueirêdo, G. Murillo-Ciordia, A. Sanz-Martinez, I.A.J. Burillo, Potentials and limitations of microwave-assisted chemical recycling of fiber-reinforced composites from wind blades, Sustain. Energy Fuels 8 (2024) 4752.
[18] J. Beauson, A. Laurent, D.P. Rudolph, J. Pagh Jensen, The complex end-of-life of wind turbine blades: a review of the European context, Renew. Sustain. Energy Rev. 155 (2022) 111847.
[19] ASTM D4752–20, Practice for Measuring MEK Resistance of Ethyl Silicate (Inorganic) Zinc-Rich Primers by Solvent Rub, ((n.d.)).
[20] ASTM D4541, Test Method for Pull-Off Strength of Coatings Using Portable Adhesion Testers, ((n.d.)).
[21] ASTM D3363, Test Method for Film Hardness by Pencil Test, ((n.d.)).
[22] X. Kuang, Q. Shi, Y. Zhou, Z. Zhao, T. Wang, H.J. Qi, Dissolution of epoxy thermosets: via mild alcoholysis: the mechanism and kinetics study, RSC Adv. 8 (2018) 1493–1502.
[23] M. Musiani, M.E. Orazem, N. Pébère, B. Tribollet, V. Vivier, Determination of resistivity profiles in anti-corrosion coatings from constant-phase-element parameters, Prog. Org. Coating 77 (2014) 2076–2083.
[24] I.C.P. Margarit-Mattos, EIS and organic coatings performance: revisiting some key points, Electrochim. Acta 354 (2020) 136725.
[25] S.A. Policastro, R.M. Anderson, C.M. Hangarter, A. Arcari, E.B. Iezzi, S.A. Policastro, R.M. Anderson, C.M. Hangarter, A. Arcari, E.B. Iezzi, Experimental and numerical investigation into the effect of water uptake on the capacitance of an organic coating, Materials 16 (2023).
[26] R.M. Souto, V. Fox, M.M. Laz, S. Gonzlez, Electrochemical impedance spectroscopy investigation of the corrosion at metallic substrates covered by organic coatings, J. Adhes. Sci. Technol. 14 (2000) 1321–1330.
[27] E. Akbarinezhad, J. Neshati, F. Rezaei, Investigation on organic pipeline coating effectiveness via electrochemical impedance spectroscopy, Surf. Eng. 23 (2007) 380–383.
[28] A. Cristoforetti, F. Deflorian, S. Rossi, M. Fedel, On the limits of the EIS low-frequency impedance modulus as a tool to describe the protection properties of organic coatings exposed to accelerated aging tests, Coatings 13 (2023) 598.
[29] M.E. Orazem, B. Tribollet, in: Electrochemical Impedance Spectroscopy, first ed., Wiley, 2008.
[30] M. Hoseinpoor, T. Prošek, L. Babusiaux, J. Mallégol, Simplified approach to assess water uptake in protective organic coatings by parallel plate capacitor method, Mater. Today Commun. 26 (2021) 101858.
[31] A. Miszczyk, K. Darowicki, Water uptake in protective organic coatings and its reflection in measured coating impedance, Prog. Org. Coating 124 (2018) 296–302.
[32] I. Kada, D. Trinh, S. Mallarino, S. Touzain, Physical ageing effect on water uptake and adhesion of epoxy coatings by EIS and the blister test, Electrochim. Acta 454 (2023) 142381.
[33] F. Spini, P. Bettini, End-of-Life wind turbine blades: review on recycling strategies, Compos. B Eng. 275 (2024).
[34] Transforming end-of-life composites into value, EuCIA, transforming end-of-life composites into value. https://eucia.eu/wp-content/uploads/2025/06/Transforming-end-of-life-composites-into-value.pdf. (Accessed 12 February 2026).
[35] World Coatings Council (WCC) & American Coatings Association (ACA), Global Market Analysis for the Paint & Coatings Industry 2024-2029, 2024. https://worldcoatingscouncil.org/. (Accessed 12 February 2026).
[36] Metal Coatings Market Size, Share & Forecast Report, Global Market Insights, 2024. https://www.gminsights.com/industry-analysis/metal-coatings-market. (Accessed 12 February 2026).
[37] World Paint and Coatings Industry Association (WPCIA), Global Paint and Coatings Industry Market Analysis (2023-2028), 2024. https://www.worldpaint.org/. (Accessed 12 February 2026).
[38] Alkyd Resin Market Size, Share & Trends Report, 2024 - 2030, Grand View Research, 2024. https://www.grandviewresearch.com/industry-analysis/alkyd-resin-market-report. (Accessed 12 February 2026).